Long-time semiclassical evolution of spinlike systems from Majorana sampling

Iván F. Valtierra [*] and Andrei B. Klimov [†]

Departamento de Fisica, Universidad de Guadalajara, 44420 Guadalajara, Jalisco, Mexico

We propose an approach to the analysis of the semiclassical evolution of spinlike systems. We show that an appropriate discretization of distributions in classical phase space (in this case the two-dimensional sphere $\mathscr{S}_2$) allows us to describe long-time dynamics (including the Schrödinger cat times) in terms of classical trajectories, both in stable and nonstable regimes and for a variety of initial states. The discretization method is based on the Majorana stellar representation of spin states and takes into account dynamical properties of the initial distribution in the corresponding classically generated potential on $\mathscr{S}_2$.

I. INTRODUCTION

The idea to employ classical language for description of quantum systems has attracted considerable attention for a long time. Such a semiclassical approach not only allows us to gain a deeper insight into the nature of quantumness, but can also be very useful for practical calculations when, due to the overwhelming complexity of macroscopic quantum states, the exact solution cannot be obtained inclusively by numerical methods [1]. The reduction of the effective dimension of a quantum dynamical system using the concept of classical propagation is a key ingredient in different types of semiclassical approximations in the configuration and momentum space and in the abstract Hilbert space [2–4]. Over the last decades several procedures were developed in order to introduce quantum nonlocality in classically motivated calculation schemes [4–8].

Unfortunately, most of the proposed methods are technically cumbersome and do not provide a clear physical and/or geometrical interpretation. Phase-space methods [9–11] offer a more natural way to analyze the quantum-classical transition both from kinematic and dynamic perspectives. In the framework of this approach every operator $\hat{f}$ is mapped into a function $W_f(\Omega)$ (the Weyl symbol) defined on the corresponding classical phase space $\mathscr{M}$, $\Omega \in \mathscr{M}$ being the phase-space coordinates. The most appropriate for applications is the self-dual (Wigner) map, when the mean values of observables are computed by convoluting the symbol of an operator with the symbol of the density matrix (the Wigner function) $W_\rho(\Omega)$. The quantum dynamics is then seen as an evolution of the Wigner function and described by a partial differential equation (the Moyal equation) generally containing higher-order derivatives.

The simplest (Liouvillian) approximation, consisting in propagating every point of the initial distribution along the corresponding classical trajectory, allows one to represent a

short-time dynamics of coherentlike states quite well. For longer times, the initial localized distribution spreads in phase space, and its evolution starts to deviate considerably from that predicted by the classical dynamics. The timescale where the classical-quantum correspondence breaks down is usually referred to as Ehrenfest (or semiclassical) time [12] t_sem. Although several improvements to Liouvillian approach, aimed to include quantum coherences, have been considered [13–15], it seems inadequate to assess the nonharmonic quantum dynamics of the Wigner function $W_\rho(\Omega|t)$ beyond the semiclassical time by assigning a single deterministic trajectory to each phase-space point [16]. Significant progress in construction of semiclassical phase-space propagators, able to describe quantum interference effects for systems evolving in flat phase space, has been recently achieved [17,18]. In this case, a particular form of the WKB solution proper to the Heisenberg-Weyl (HW) symmetry and accounting a coherence between several trajectories was used. The quantum systems with higher symmetries are considerably less scrutinized on the subject of long-time semiclassical evolution [19].

In spite of the intrinsic problems with the Liouvillian approximation, the estimation of average values according to

$$\langle \hat{f}(t) \rangle \approx \int d\Omega \, W_f(\Omega^{cl}(t)) W_\rho(\Omega), \tag{1.1}$$

where $\Omega^{cl}(t)$ denotes the classical trajectories, has been widely applied for the analysis of semiclassical dynamics of quantum systems with the Heisenberg-Weyl [2,20] (see also [15] and references therein), SU(2) [21,22] and SU(3) symmetries [22,23]. The approximation (1.1), usually called the truncated Wigner approximation (TWA), leads to exact results for the harmonic evolution. In the nonharmonic case TWA describes relatively well only a short-time behavior of low-order correlation functions for initial smooth and localized distributions (representing the so-called semiclassical states) in stable dynamical regimes. It was detected [14] that direct improvements of TWA not only require considerable numerical efforts, but also do not substantially increase the accuracy of the approximation.

───────

[*]fernando11.valtierra@gmail.com

[†]Corresponding author: klimov@cencar.udg.mx

It is clear that statistically independent (noncorrelated) classical trajectories originated at every point of the initial distribution produce only a destructive dynamic interference when the average values are computed according to Eq. (1.1). Indeed, in stable nonharmonic regimes the integration of rapidly oscillating functions, where the period of oscillations inversely depends on the effective dimension of the system, may lead to an acceptable description only of the initial stage of evolution (in the best case the collapse but never the revival). In unstable configurations even the first oscillation of $\langle \hat{f}(t) \rangle$ is usually not described by the prescription (1.1). In addition, integrating $W_f(\Omega^{cl}(t))$ with the initial distribution one assumes that even infinitesimally close phase-space points are classically distinguishable at any time (since there is no trajectory crossing).

One of the proposals to emulate quantum evolution of certain observables beyond semiclassical times by using the idea of propagation along classical trajectories consists in a discrete sampling of initial phase-space distributions. In general, it is not obvious if it is possible to find such a phase-space discretization so that the classical trajectories started only at appropriate points of the initial distribution constructively interfere and produce results consistent with quantum calculations. For instance, it was suggested in [24] that an ensemble of classical trajectories with a single one for a Planck cell may describe certain quantum interference effects in the semiclassical limit. In a similar vein, the discrete Wigner function formalism [25] was employed in order to extend TWA to N-partite $\frac{1}{2}$-spin systems [26]. The discrete TWA (DTWA) method, based on a classical evolution of distributions sampled in a discrete phase space, has been recently successfully applied for semiclassical description of Ising-type chains dynamics [26,27]. Unfortunately, the intrinsic problem of the DTWA scheme related to the determination of optimal sampling of initial states may significantly restrict the range of its applications, especially for finding the long-time behavior [28].

Here, we propose an alternative approach to the problem of semiclassical description of phase-space dynamics focusing on spinlike systems in the limit of large spin length $S \gg 1$. We will introduce a method of dynamical discretization which allows us to sample the Wigner function of the initial state for a given Hamiltonian, so that the long-time behavior of physical observables can be computed in terms of classically evolved quantities. We will show that a faithful discrete sampling of a variety of initial distributions can be performed by employing the Majorana description [29] of quantum states. Specifically, a short-time dynamics of the Majorana points corresponding to an initial (pure) state leads to a constellation which, if mapped appropriately to an initial Wigner distribution, describes the latter one with high accuracy. Moreover, the classical trajectories originated in these projected Majorana points are used for the simulation of the quantum evolution of mean values. It will be shown that such an approach leads to drastically better results than the TWA solution, especially in unstable dynamical configurations, i.e., when the initial distribution is located in a neighborhood of unstable fixed points (of an integrable system).

We do not attempt to describe the entire quantum state dynamics, but instead we will be interested in the evolution of the lowest moments of spin observables for timescales where quantum interference effects have already manifested. In addition, it will be shown that only a small number of sampling points $\sim S$ suffice to describe dynamics of spin observables for a variety of initial (not necessarily semiclassical) states and governing Hamiltonians. Here, we consider only time-independent second order on spin operator Hamiltonians, which commonly appear in physical applications.

II. MAJORANA DISCRETIZATION

For spinlike systems, where the classical manifold is the $\mathscr{S}_2$ sphere, the standard tracelike map [30] from operators acting in the Hilbert space, spanned by the angular momentum basis $\{|S, k\rangle, \; k = -S, \ldots, S\}$, into distributions on the $\mathscr{S}_2$ sphere

$$\hat{f} \Leftrightarrow W_f(\Omega) = \mathrm{Tr}(\hat{f}\,\hat{\omega}(\Omega)), \quad \Omega = (\theta, \phi) \in \mathscr{S}_2, \quad (2.1)$$

is generated by the kernel

$$\hat{\omega}(\Omega) = \sqrt{\frac{4\pi}{2S+1}} \sum_{L=0}^{2S} \sum_{M=-L}^{L} Y_{LM}^*(\Omega)\hat{T}_{LM}^S, \quad (2.2)$$

where $Y_{LM}(\Omega)$ are the spherical harmonics and $\hat{T}_{LM}^S$ are the irreducible tensor operators [31].

In the *semiclassical limit* corresponding to large spins $S \gg 1$, the Liouvillian equation

$$\partial_t W_f(\Omega) \approx \epsilon \{W_f(\Omega), W_H(\Omega)\}_P, \quad \epsilon = (S + 1/2)^{-1} \quad (2.3)$$

where

$$\{\ldots, \ldots\}_P = \frac{1}{\sin\theta}(\partial_\phi \otimes \partial_\theta - \partial_\theta \otimes \partial_\phi) \quad (2.4)$$

are the Poisson brackets on $\mathscr{S}_2$ and $W_H(\Omega)$ is the Weyl symbol of the Hamiltonian, describes the (classical) evolution of the distribution

$$W_f(\Omega) \Rightarrow W_f(\Omega|t) \approx W_f(\Omega^{cl}(t)),$$

$\Omega^{cl}(t)$ being the corresponding classical trajectories.

Let us consider a discretized form of the kernel (2.2), which is determined by a set of points on the sphere (a sampling set) $\{\Omega_j, j = 1, \ldots, N\}$,

$$\hat{\omega}^d(\Omega) = \frac{4\pi}{2S+1}\lambda \sum_j \hat{\omega}(\Omega_j)\delta(\Omega, \Omega_j), \quad (2.5)$$

where

$$\delta(\Omega, \Omega') = \sum_{LM} Y_{LM}^*(\Omega)Y_{LM}(\Omega')$$

is the delta function on the sphere. The discretized kernel (2.5) satisfies the normalization condition

$$\lambda \sum_j \hat{\omega}^d(\Omega_j) = 1, \quad (2.6)$$

where the constant λ will be defined later.

The main approximation consists in propagating the *discretized* symbols of physical observables

$$W_f^d(\Omega) = \mathrm{Tr}(\hat{f}\,\hat{\omega}^d(\Omega))$$

along classical trajectories $\Omega^{cl}(t)$, so that the average values, computed according to Eq. (1.1), are recast as follows:

$$\langle \hat{f}(t) \rangle = \lambda \sum_j W_\rho^d(\Omega_j) W_f^d\left(\Omega_j^{cl}(t)\right), \qquad (2.7)$$

where $\Omega_j^{cl}(t)$ indicates trajectories originated at the sampling points $\{\Omega_j\}$.

The choice of the optimal set of sampling points is a commonly arising problem in the field of state estimation. The sampling sets are usually determined from algebraical and/or geometrical considerations, imposing the condition that the homogeneous functions (on a given manifold), evaluated at the elements of the set, constitute a specific basis allowing estimation of certain types of correlation functions (i.e., $\{\Omega_j\}$ form appropriate t designees [32,33]).

Unfortunately, such an approach results inefficient in the framework of simulation of quantum evolution through classical propagation since the dynamic properties of the initial distribution, generated by a given Hamiltonian, are not taken into account. The dynamic characteristics of trajectories (e.g., the stability of the classical motion) are, however, very important and strongly reflected in the corresponding quantum dynamics. For instance, the semiclassical time for a stable (nonlinear) evolution of spin coherent states on the $\mathscr{S}_2$ sphere is $\chi t_{\text{sem}} \sim \epsilon^{1/2}$, while in the unstable integrable case $\chi t_{\text{sem}} \sim \epsilon$ [34], where χ is a coupling constant that determines the timescale of the nonlinear evolution.

The idea of dynamical discretization comes from the following observation. Any pure spin state $|\psi\rangle$ is completely defined by its Majorana stellar representation [29,35,36] through the points on the two-dimensional sphere $\{z_j, j = 1, \ldots, 2S\}$, which are zeros of the Q function,

$$Q(\Omega) = |\langle \Omega | \psi \rangle|^2 \sim \Pi_j [z(\Omega) - z_j],$$
$$z(\Omega) = \cot \frac{\theta}{2} e^{i\phi}, \qquad (2.8)$$

where $|\Omega\rangle$ stands for the spin coherent state.

For an initial coherent state $|\Omega_0\rangle$ there is just a single $2S$-degenerated Majorana point $Q_0(\Omega) \sim |z - z_0|^{2S}$. Under the action of a nonlinear Hamiltonian this single point is rapidly split into $2S$ points spread over the sphere

$$Q(\Omega|t) \sim \Pi_j[z - z_j(t)].$$

The time-evolved position $z_j(t)$ on the sphere depends both on the location of the distribution corresponding to $|\Omega_0\rangle$ inside the potential generated by the symbol of the Hamiltonian $W_H(\Omega)$, and on the degree of nonlinearity of the Hamiltonian. The Hamiltonians linear on the angular momentum operator produce just a solid rotation of the initial distribution, i.e.,

$$Q_0(\Omega|t) \sim |z - z_0(t)|^{2S}.$$

It turns out that already for short times $\chi t \sim S^{-1}$, the antipodal Majorana points, i.e.,

$$\alpha_j(t) = -1/z_j^*(t), \qquad (2.9)$$

partially cover the initial distribution [observe that the maximum of $Q(\Omega|0)$ is reached at the point $\alpha_0 = -1/z_0^*$ for an initial spin coherent state]. From now on, we will use the notation τ for times corresponding to the initial stage of quantum

evolution, i.e., for the timescales $\chi \tau \sim S^{-1}$. Our main idea consists of using the Majorana points (2.8) and (2.9) to sample the initial Wigner distribution

$$W_\rho(\Omega) \to W_\rho^d(\Omega_j(\tau)),$$

where

$$\{\Omega_j(\tau)\} \Leftrightarrow \left\{ \alpha_j(\tau) = -\tan \frac{\theta_j}{2} e^{i\phi_j} \right\}. \qquad (2.10)$$

The sampling time τ_s, $\{\Omega_j(\tau_s)\} \Leftrightarrow \{\alpha_j(\tau_s)\}$, determining the configuration of the sampling set optimal for the classical simulation (2.7) can be obtained by imposing the condition of the best sampling of the initial distribution $W_\rho(\Omega)$ by $\{\Omega_j(\tau_s)\}$, i.e., by maximizing the fidelity (the normalized overlap between the distribution and its discrete sampling)

$$\mathscr{F}(\tau) = \frac{2S+1}{4\pi} \int d\Omega \, W_\rho(\Omega) W_\rho^d(\Omega|\tau)$$
$$= \lambda \sum_j W_\rho^2(\Omega_j(\tau)), \qquad (2.11)$$

so that

$$\max \mathscr{F}(\tau) = \mathscr{F}(\tau_s). \qquad (2.12)$$

We stress that here $\Omega_j(\tau)$ indicates the (exact) quantum dynamics of the antipodal Majorana points, which play the role of "seeds" for the consecutive classical evolution $\Omega_j^{cl}(t)$.

Obviously, only those points $\{\Omega_j(\tau_s), \ j = 1, \ldots, N\}$ that are located inside the principal part of the initial Wigner distribution [i.e., inside the phase-space area $A(\Omega)$ describing fluctuations of the spin variables] significantly contribute to the sampling. This allows us to estimate the normalization constant λ from the condition

$$\lambda \sum_{j=1}^N W_\rho^d(\Omega_j(\tau_s)) = 1, \qquad (2.13)$$

which follows from Eq. (2.6). Actually,

$$\lambda^{-1} \approx N\bar{W}_\rho(\Omega),$$
$$\bar{W}_\rho(\Omega) = [W_\rho(\Omega_0) + W_\rho(\Omega_N)]/2, \qquad (2.14)$$

Ω_N being a border point of $A(\Omega)$, is an excellent approximation for the coherent states where at the maximum of the distribution $W_\rho(\Omega_0) = 2$.

In general, the dynamics of Majorana points is described by a system of nonlinear differential equations, which exact solution is a nontrivial task [37]. Nevertheless, in the case of initial semiclassical states with $A(\Omega) \sim S$, e.g., spin coherent states, the situation is significantly simplified for short-time dynamics of the points $\{\alpha_j(\tau), \ j = 1, \ldots, N\}$ such that

$$\alpha_j(\tau) = \alpha_0[1 + \mu_j(\tau)], \quad |\mu_j(\tau)| \sim S^{-1/2}, \qquad (2.15)$$

where $z_0 = -1/\alpha_0^*$ is a Majorana point characterizing the initial Q distribution. Below, we will show particular examples where $\{\mu_j(\tau)\}$ satisfies some approximate equations of motion which can be solved analytically.

A discrete Majorana sampling can be performed not only for localized functions on $\mathscr{S}_2$ (describing coherentlike states), but also for a variety of initial distributions including nonlocalized states (e.g., Dicke state) and squeezed states. The
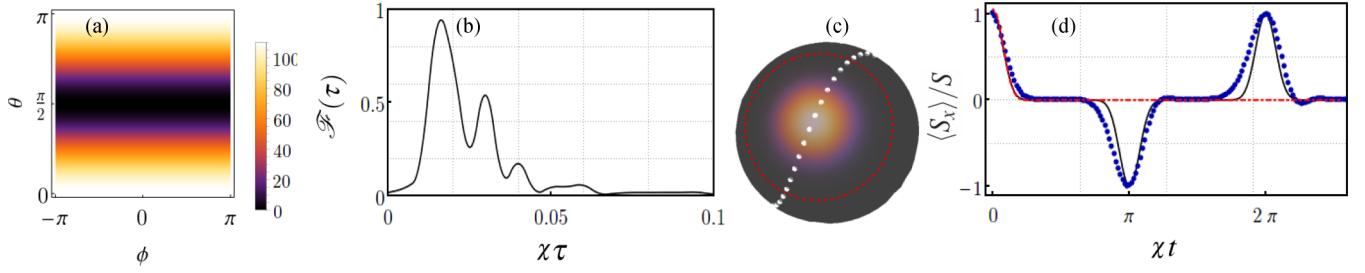
FIG. 1. (a) Density plot of the classical potential (3.2) generated by the Hamiltonian (3.1); (b) evolution of the fidelity (2.11) corresponding to the sampling points (3.4); (c) distribution of the Majorana points at the best sampling time τ_s; (d) evolution of $\langle \hat{S}_x(t) \rangle$. Exact dynamics (black solid line), the dynamically discretized TWA (blue dotted line), and the standard TWA (red dotted-dashed line); $S = 10$.

map from the Majorana points $\{z_j(\tau)\}$ onto points inside the distribution could be more involved than for the coherent spin states, but the optimization procedure, described by the maximization of $\mathscr{F}(\tau)$, remains the same. It turns out that the sampling time is very short for nonlocalized distributions too, $\chi \tau_s \sim S^{-1}$.

It is worth noting that the distribution of the Majorana points were numerically analyzed for studying classically chaotic quantum systems [36].

III. EXAMPLES

A. Kerr dynamics

The finite Kerr Hamiltonian

$$\hat{H}_z = \chi \hat{S}_z^2 \tag{3.1}$$

generates the simplest nonlinear evolution where such physical effects as spin squeezing [38] and the Schrödinger cat states [39] naturally emerge. The symbol of the Hamiltonian (3.1),

$$W_H(\Omega) \simeq \chi \epsilon^{-2} \cos^2 \theta, \tag{3.2}$$

corresponds to a potential valley on the equator [see Fig. 1(a)] of the sphere and allows us to find an analytical expression for the classical trajectories leading to the following discretized TWA solution:

$$\langle \hat{f}(t) \rangle = \lambda \sum_j W_\rho^d(\Omega_j) W_f^d(\theta_j, \phi_j - 2\epsilon^{-1} \chi t \cos \theta_j). \tag{3.3}$$

For the initial spin coherent state located on the equator $|\theta = \pi/2, \varphi = 0\rangle$, the sampling points are (see Appendix)

$$\theta_j \approx \pi/2 + \sqrt{2} \chi \tau \nu_j, \quad \phi_j \approx (\sqrt{2} \nu_j - 1) \chi \tau, \tag{3.4}$$

where ν_j are zeros of the Hermite polynomial $H_{2S}(\nu_j) = 0$. The optimal sampling time corresponds to the first maximum of the fidelity (2.11) [see Fig. 1(b)], where $\chi \tau_s \sim 0.021$ for $S = 10$. The number of sampling points inside the coherent state area, which is always taken as 3σ of the standard quantum spin noise, scales as $N \sim S^{0.4}$. In Fig. 1(c) we show the distribution of the Majorana points at the best sampling time $\chi \tau_s \sim 0.021$. Only the points inside the (red) circle contribute to the sampling of the initial coherent state.

In Fig. 1(d) we plot the evolution of $\langle \hat{S}_x(t) \rangle$ obtained from Eq. (3.3) and compare with the exact dynamics and the standard TWA; while the standard TWA fails at $\chi t \sim S^{-1/2}$

(and does not reproduce even the first revival at $\chi t = \pi$) the dynamically discretized TWA (DDTWA) exhibits a very good agreement with the results of the exact calculations for times far beyond the first revival. Evolution of other observables and different initial states is discussed in Sec. IV.

B. Lipkin-Meshkov-Glik dynamics

As an example of unstable evolution we consider the Lipkin-Meshkov-Glik (LMG) Hamiltonian [40]

$$\hat{H} = -h\hat{S}_x + \frac{\lambda}{2(2S+1)} (\hat{S}_z^2 - \hat{S}_y^2). \tag{3.5}$$

The main interesting feature of this model is a presence of the quantum phase transition at $\lambda = h/2$. In the undercritical regime $\lambda < h/2$, where the energy levels are well separated, there are two types of classical trajectories corresponding to oscillations inside a single potential well with the minimum at $(\theta = \pi/2, \phi = 0)$ and "rotations" outside the well. In the critical regime $\lambda = h/2$, only oscillations remain and after the phase transition point $\lambda > h/2$ the energy levels become degenerated, the oscillation areas are separated by local maxima.

We will be interested in the unstable regime $\lambda > h/2$, when the potential on the sphere described by the Weyl symbol

$$W_H(\Omega) \approx -(2\epsilon)^{-1} [h \sin \theta \cos \phi + \lambda \sin^2 \theta (1 + \sin^2 \phi)] \tag{3.6}$$

consists of two minima separated by local maxima [see Fig. 2(a)] and the classical trajectories can be expressed in terms of elliptic functions [41]. This Hamiltonian is integrable but not exactly solvable and is characterized by a nontrivial phase-space evolution significantly different from that of the Kerr dynamics. It is worth noting that the nonlinear part of the Hamiltonian (3.5) is equivalent to the so-called two-axis squeezing Hamiltonian $H = \xi(\hat{S}_z^2 - \hat{S}_y^2) = 2\xi\{\hat{S}_x, \hat{S}_y\}_+$ [38], under $\pi/4$ rotation around the z axis.

The distribution corresponding to the initial spin coherent state $|\pi/2, 0\rangle$ is centered at one of the local maxima (in the vicinity of the classical separatrix) and leads to the classically unstable motion. For this initial state the sampling points are (see Appendix)

$$\theta_j \approx \frac{\pi}{2} + \text{Re}(e^{-i\beta\tau} 2\sqrt{2i\gamma\tau}\sqrt{1 - i\beta\tau}\nu_j), \tag{3.7}$$

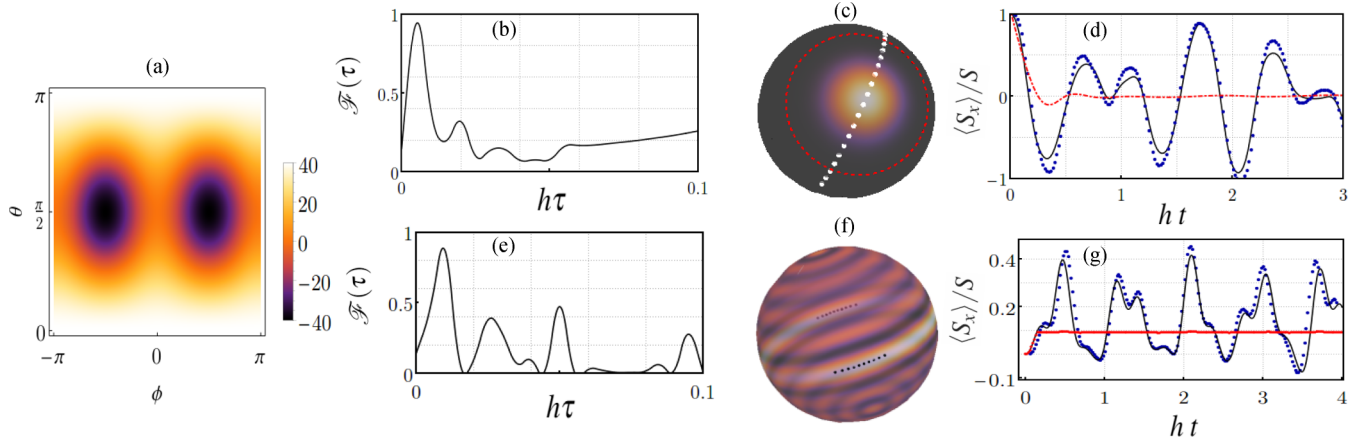$$\phi_j \approx \text{Im}(e^{-i\beta\tau} 2\sqrt{2i\gamma\tau}\sqrt{1 - i\beta\tau}\nu_j), \tag{3.8}$$

FIG. 2. (a) Density plot of the classical potential (3.6) generated by the Hamiltonian (3.5) with $\lambda = 30$; (b) evolution of the fidelity (2.11) for the sampling points (3.7) and (3.8); (c) distribution of the Majorana points at the best sampling time $\tau_s = 0.0095$; (d) evolution of $\langle \hat{S}_x \rangle$ for the coherent state $|\pi/2, 0\rangle$; (e) evolution of the fidelity for the initial Dicke state $|S, 0\rangle$; (f) distribution of the Majorana points at the best sampling time $\tau_s = 0.0005$; (g) evolution of $\langle \hat{S}_x \rangle$ for the Dicke state $|S, 0\rangle$. Exact evolution (black solid line), the DDTWA (blue dotted line), and the standard TWA (red dotted-dashed line); $S = 10$.

where $\beta = \frac{\lambda(2s-1)}{2(2s+1)} - h$, $\gamma = \frac{\lambda}{2(2s+1)}$, and $H_{2S}(\nu_j) = 0$ (as in the Kerr case). The optimal sampling time corresponding to the first maximum of the fidelity (2.11) [see Fig. 2(b)] is slightly shorter than in the Kerr case $\gamma \tau_s \sim 0.0095$ for $S = 10$. The number of sampling points inside the coherent state area $A(\Omega)$ scales as $N \sim S^{0.5}$ [see Fig. 3(a)] and their distribution is similar to that of the Kerr medium [see Fig. 2(c)], although the analytical expressions (3.7) and (3.8) are quite different.

In Fig. 2(d) we plot the evolution of $\langle S_x(t) \rangle$ along with the exact and the standard TWA. One can observe that the DDTWA (2.7), (2.10), and (2.12) describe very well the exact dynamics even for long times in the deeply unstable regime $\lambda = 30$, while the standard TWA fails at very short times $\gamma t \sim S^{-1}$ [34].

As a remarkable application of the present approach, we study the evolution of the initial angular momentum state with zero projection to the z axis $|0, S\rangle$, which is equivalent to the Dicke state with S among $2S$ excited two-level atoms. The Wigner function of this state has the form of a narrow belt on the equator of the sphere, i.e., it is completely delocalized. The state $|0, S\rangle$ is an "opposite" to a semiclassical state and the standard TWA usually does not describe even short-time nonharmonic dynamics.
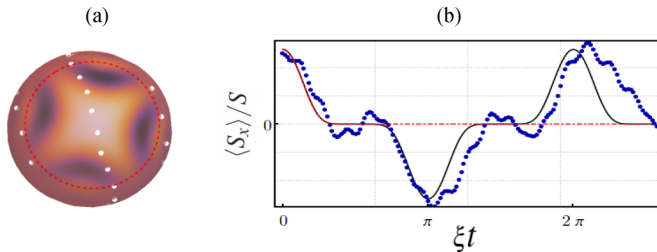

FIG. 3. (a) The distribution corresponding to the squeezed state $e^{-0.5i(S_+^2 - S_-^2)}|\pi/2, 0\rangle$; (b) evolution of $\langle S_x \rangle$ generated by the two-axis Hamiltonian, exact evolution (black solid line), DDTWA (blue dotted line), and the standard TWA (red dotted-dashed line); $S = 10$.

The corresponding Majorana constellation consists in two S-times degenerated points at the north and south poles. Under the action of the Hamiltonian (3.5), the Majorana points $z_j = z(\theta_j, \phi_j)$ for short times spread in small vicinities of both poles:

$$(\theta = 0, \phi = 0) \Rightarrow (\theta_j^+(\tau), \phi_j^+(\tau); \ j = 0, \dots, S),$$

$$(\theta = \pi, \phi = 0) \Rightarrow (\pi - \theta_j^-(\tau), \phi_j^-(\tau); \ j = S, \dots, 2S),$$

where $\theta_j^{\pm}(\tau) \ll 1$. The sampling set in this case is obtained by a direct projection of the Majorana points at $\gamma \tau \sim S^{-1}$ onto the initial distribution by preserving the angles $\phi_j^{\pm}(\tau)$:

$$\{\alpha_j^+(\tau)\} \Leftrightarrow (\pi/2, \phi_j^+(\tau); \ j = 0, \dots, S), \tag{3.9}$$

$$\{\alpha_j^-(\tau)\} \Leftrightarrow (\pi/2, \phi_j^-(\tau); \ j = S, \dots, 2S). \tag{3.10}$$

The optimal sampling time is significantly shorter for the state $|0, S\rangle$ in comparison with an initial coherent state: the maximum fidelity (2.11) is reached at $\chi \tau_s \sim 0.0005$ for $S = 10$ [see Fig. 2(e)]. It is worth noting that in contrast to the coherent state, *all* the Majorana points are required for a good sampling of Dicke states. In Fig. 2(f) we show the distribution of the Majorana points at the best sampling time.

The normalization constant λ, evaluated according to Eq. (2.13) with $N = 2S$, can be also estimated from Eq. (2.14) as $\lambda^{-1} \approx 2S$, since the value of the Wigner function at the maximum of the distribution (on the equator) is 1.

In Fig. 2(d) the exact evolution of $\langle \hat{S}_x(t) \rangle$ is plotted along with the discretized TWA and compared to the standard TWA (which does not describe even the initial stage of the evolution). A similar procedure can be carried out for any other Dicke state $|S, m\rangle$, whose Majorana constellation consists of $S + m$ degenerate points on the north pole and $S - m$ degenerate points on the south pole, while the Wigner function for $m \neq \pm S$ has the form of a ring on the sphere around the z axis.

The general form of the map $z \to \alpha = F[z]$ from the Majorana points $z_j(t)$ in the vicinity of poles onto the distributions

corresponding to the states $|S, m\rangle$, $-S \leqslant m \leqslant S$ is

$$F[z] = \frac{|z|(|z|z_0 - 1)}{z^*(|z| + z_0)}, \quad z_0 = \cot\left(\pi \frac{m+S}{4S}\right). \quad (3.11)$$

For instance, the map (3.9) and (3.10) corresponds to $z_0 = 1$, i.e.,

$$\alpha_j = \frac{\cot\theta_j/2 - 1}{\cot\theta_j/2 + 1} e^{i\phi_j}.$$

Dicke states in any other basis are sampled by applying a corresponding Mobius transformation to the map (3.11).

IV. DISCUSSION

We have shown that the long-time, $\chi t \lesssim S^\alpha$, $\alpha > 0$, non-linear evolution of some spin observables can be described in terms of classical trajectories originated at appropriately chosen phase-space points. It is worth noting that the semi-classical approximations based on statistically independent classical trajectories in general do not lead to a faithful representation of the long-time evolved Wigner function since the classical dynamics preserves the phase-space area and thus fails to describe any properly quantum deformations of the initial phase-space distribution [16], for instance its splitting.

Thus, an efficient emulation of the quantum interference effects, reflected in a close resemblance to the exact and approximate calculations [Eq. (2.7)], should be attributed to a suitable discretization of the initial phase-space distribution. Actually, the form of the employed *dynamical* discretization plays the crucial role in our framework. Such a discretization is obtained from a systematic procedure involving an analytical description of the short-time quantum dynamics in terms of Majorana point evolution. The discrete sampling is performed by mapping the evolved Majorana points $z_j(t)$ to the initial Wigner function. For localized distribution, such a map is just $F[z] = -1/z^*$, while for nonlocalized ones the map may acquire more sophisticated form, as for instance, Eq. (3.11) for Dicke states. The proposed discretization method provides good results, i.e., close to unity overlap between the Wigner distribution and its discretized sampling, when the Q and Wigner functions are of similar form. For instance, the Majorana sampling does not work for superpositions of strongly interfering states, e.g., catlike states (superposition of two distant coherent states), where the interference term in the Wigner function is significantly larger than the corresponding term in the Q function.

In a sense, the classical trajectories used for the simulation of the interference pattern start at the points forming a "correlated set," while all the other trajectories are disregarded. We emphasize that the number of sampling points $N \sim S^a$, $a \leqslant 1$, required for the simulation of quantum dynamics is significantly smaller than that used in other semiclassical calculation schemes, for instance, in the DTWA [26,27].

We have performed extensive numerical simulations applying our method to different initial states and observables in case of second degree on the spin-operator Hamiltonians. We obtained that the evolution of the first-order moments are well described for initial coherentlike states (deformations of coherent states) and Dicke states in different bases (i.e.,
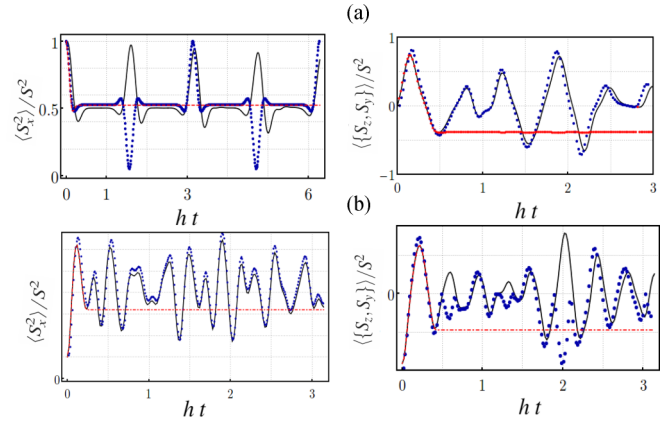

FIG. 4. Evolution of $\langle \hat{S}_x^2(t) \rangle$ and $\langle \{\hat{S}_z, \hat{S}_y\}_+(t) \rangle$ corresponding to the LMG dynamics (3.5), for (a) the initial coherent state $|\pi/2, 0\rangle$; (b) the coherent state $|\pi/2, 3\pi/4\rangle$ exact evolution (solid line), the DDTWA (dotted line), and the standard TWA (dotted-dashed line); $S = 10$.

eigenstates of $\hat{S}_{x,y,z}$ operators). In case of more "sophisticated" initial states, represented by nonsmooth distributions on the sphere, the main features of the evolution are still grasped in the present approach [see Fig. 3 where we plot the evolution of $\langle \hat{S}_x(t) \rangle$ for an initial spin coherent state (maximally) squeezed by the action of the two-axis Hamiltonian].

The situation becomes more delicate with higher-order moments. In general, the results obtained from the proposed method fit well with the exact calculations for a wide variety of initial states. The DDTWA shows a partial discrepancy with the exact evolution of observables $\hat{L}(t)$ that can detect two-component superpositions of coherentlike states (Schrödinger
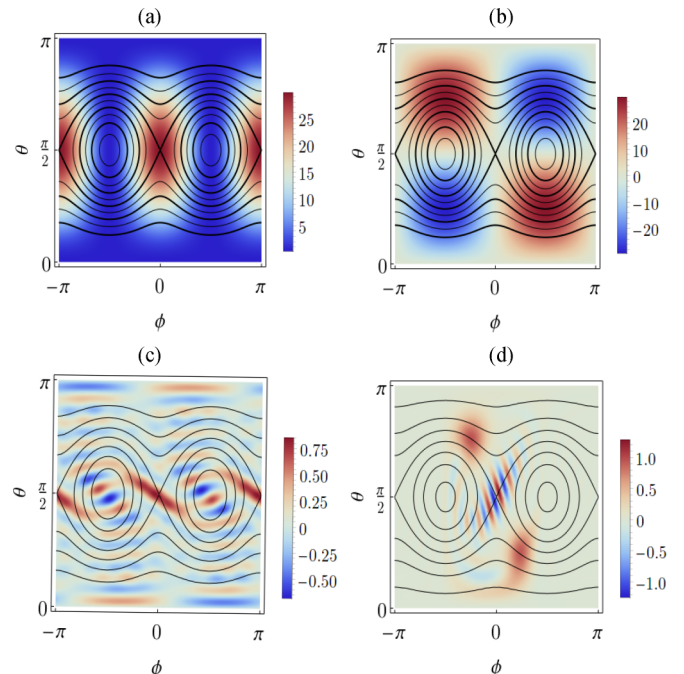

FIG. 5. Density plot of the Weyl symbols: (a) $W_{\hat{S}_x^2}(\Omega)$; (b) $W_{\{\hat{S}_z, \hat{S}_y\}_+}(\Omega)$ and the Weyl symbols (c) $W_{|\pi/2,0\rangle}(\Omega(t = \pi/2))$; (d) $W_{|\pi/2,3\pi/4\rangle}(\Omega(t = 2.08))$, in the potential (3.6) represented by black contour lines.
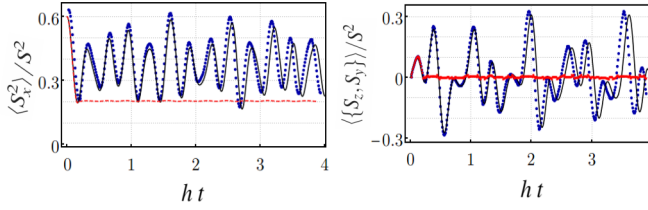
FIG. 6. Evolution of $\langle S_x^2(t) \rangle$ and $\langle \{\hat{S}_z, \hat{S}_y\}_+(t) \rangle$ for the initial Dicke state $|S, 0\rangle$ corresponding to the LMG dynamics (3.5), exact evolution (black solid line), the DDTWA (blue dotted line), and the standard TWA (red dotted-dashed line); $S = 10$.

FIG. 8. (a) Evolution of $\langle S_x^2(t) \rangle$ and (b) $\langle \{S_z, S_y\}_+(t) \rangle$ for the initial coherent state $|\pi/2, 0\rangle$ generated by the Hamiltonian (4.1), exact evolution (black solid line), the DDTWA (blue dotted line), and the standard TWA (red dotted-dashed line); $S = 10$.

cat states) generated in the course of quantum evolution, which are unattainable from the independent trajectory-based approach. Such observables are of even order on the spin operators and are represented in phase space by two humps that have a substantial overlap with the distribution representing the initial state. The observables of the described form seem to distinguish between quantum and classical deformations of phase-space distributions. This is reflected in periodical "flipping" of some peaks of mean values $\langle \hat{L}(t) \rangle$. The low *odd*-order moments of spin observables are always described by our method.

In Fig. 4 we plot $\langle \hat{S}_x^2(t) \rangle$ and $\langle \{\hat{S}_z, \hat{S}_y\}_+(t) \rangle$ for the initial spin coherent states $|\pi/2, 0\rangle$ and $|\pi/2, 3\pi/4\rangle$ corresponding to the LMG dynamics (3.5).

As one can observe, the "flips" occur for $\langle \hat{S}_x^2(t) \rangle$ at precisely the two-component cat time for the distribution located at $(\theta = \pi/2, \varphi = 0)$, while a similar behavior is present in $\langle \{\hat{S}_z, \hat{S}_y\}_+(t) \rangle$ evolution for the distribution centered at $(\theta = \pi/2, \varphi = 3\pi/4)$.

In Fig. 5 we plot the Weyl symbols of both observables at $t = 0$ in the potential (3.6) compared with the evolved Wigner function of the states $|\theta = \pi/2, \varphi = 0\rangle$ and $|\theta = \pi/2, \varphi = 3\pi/4\rangle$ at the times of the most pronounced flips $t = \pi/2$ and 2.08, respectively. The maxima of the symbol $W_{S_x^2}(\Omega)$ coincide with the positions of the maxima of the distribution $W_{|\pi/2,0\rangle}(\Omega|t)$ at $t = \pi/2$.

The symbol of the operator $\{\hat{S}_z, \hat{S}_y\}_+$ never has such a strong overlap with two-component superpositions appearing during the LMG evolution. The situation is reversed for the initial state $|\theta = \pi/2, \varphi = 3\pi/4\rangle$, where the operator $\{\hat{S}_z, \hat{S}_y\}_+$ is sensitive to the emerging of coherent superposi-
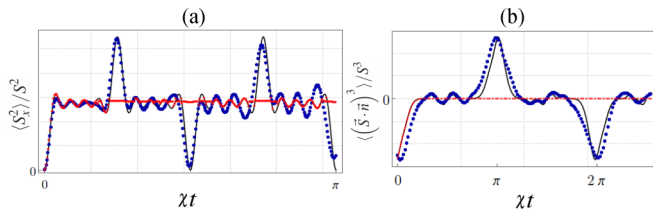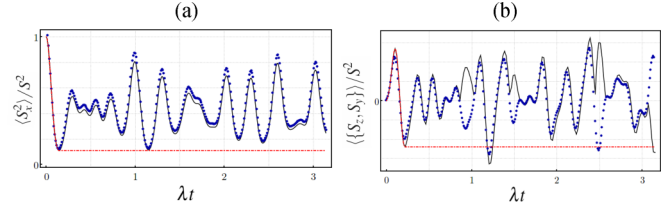
tions through the overlap of $W_{\{S_z, S_y\}_+}(\Omega)$ with $W_{|\pi/2,3\pi/4\rangle}(\Omega|t)$, as can be appreciated from Figs. 5(b) and 5(d).

The dynamics of the same observables for the initial Dicke state are well described. No pronounced superpositions of coherentlike states are generated by (3.5) for such an initial nonlocalized distribution. In Fig. 6 we plot $\langle \hat{S}_x^2(t) \rangle$ and $\langle \{\hat{S}_z, \hat{S}_y\}_+(t) \rangle$ for the initial Dicke state $|S, 0\rangle$.

Finally, we plot results of miscellaneous calculations corresponding to evolution of higher-order moments for different states and Hamiltonians:

(a) Kerr dynamics, Fig. 7(a): $\langle \hat{S}_x^2(t) \rangle$ for the initial Dicke state $|S, 0\rangle_x = e^{-i\frac{\pi}{2}\hat{S}_y}|S, 0\rangle$ in the x basis, $\hat{S}_x|S, 0\rangle_x = 0$; Fig. 7(b): evolution of the third-order moment $\langle (\hat{\mathbf{S}} \cdot \mathbf{n})^3(t) \rangle$, $\mathbf{n}(\theta = \pi/2, \varphi = 2.7)$ for an initial coherent state $|\pi/2, 0\rangle$.

(b) The evolution of $\langle \hat{S}_x^2(t) \rangle$ and $\langle \{\hat{S}_z, \hat{S}_y\}_+(t) \rangle$ for the initial coherent state $|\pi/2, 0\rangle$ in case of mixed nonlinear dynamics generated by

$$\hat{H} = \lambda \hat{S}_z^2 - 0.75i\lambda(\hat{S}_+^2 - \hat{S}_-^2), \tag{4.1}$$

are plotted in Figs. 8(a) and 8(b).

(c) The evolution of $\langle \hat{S}_x^2(t) \rangle$ and $\langle \{\hat{S}_z, \hat{S}_y\}_+(t) \rangle$ for the initial coherent state $|\pi/2, 0\rangle$ and nonlinear (Kerr dominated) dynamics generated by

$$\hat{H} = 10\lambda \hat{S}_z^2 - 0.75i\lambda(\hat{S}_+^2 - \hat{S}_-^2), \tag{4.2}$$

are plotted in Figs. 9(a) and 9(b). A remarkable description of a fast oscillating nonlinear evolution can be observed. The appearance of some flips on the plots can be explained according to the previous discussion: the dominant nonlinear term in the Hamiltonian fixes the observable where the "flip failure" is present for a given initial state. Observe that in both cases the DDTWA present the first failure at times significantly longer than the semiclassical times $\chi t_{sem} \sim S^{-a}$, $a > 0$, where the standard TWA is in general applicable.

Finally, we note that the dynamics of average values computed *exactly* in terms of the evolved phase-space distributions are perfectly described by the Majorana discretization method

$$\langle \hat{f}(t) \rangle = \lambda \sum_j W_\rho^d(\Omega_j) W_f^d(\Omega_j|t),$$

where

$$W_f(\Omega|t) = \text{Tr}(\hat{f}(t)\hat{\omega}(\Omega))$$

is the Weyl symbol of the Heisenberg operator $\hat{f}(t)$.

FIG. 7. (a) Evolution of $\langle S_x^2(t) \rangle$ for the initial state $|S, 0\rangle_x = e^{-i\frac{\pi}{2}\hat{S}_y}|S, 0\rangle$; (b) evolution of $\langle (\hat{\mathbf{S}} \cdot \mathbf{n})^3(t) \rangle$, $\mathbf{n}(\theta = \pi/2, \varphi = 2.7)$ for an initial coherent state generated by the Kerr Hamiltonian (3.1); exact evolution (black solid line), the DDTWA (blue dotted line), and the standard TWA (red dotted-dashed line); $S = 10$.
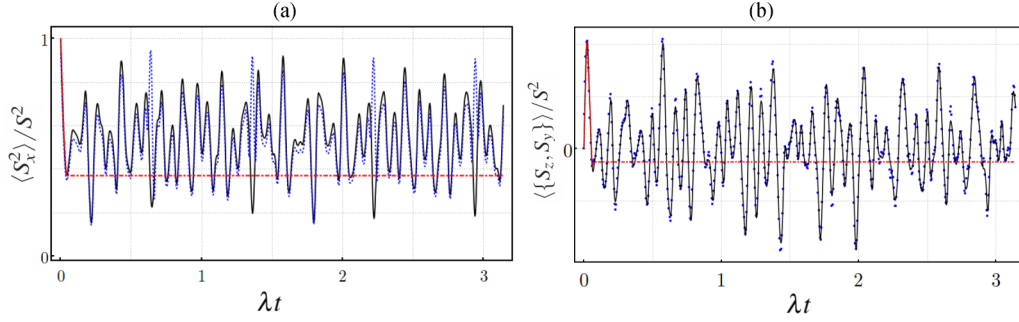
FIG. 9. (a) Evolution of $\langle S_x^2(t)\rangle$ and (b) $\langle\{S_z, S_y\}_+(t)\rangle$ for the initial coherent state $|\pi/2, 0\rangle$ generated by the the Hamiltonian (4.2), exact evolution (black solid line), the DDTWA (blue dotted line), and the standard TWA (red dotted-dashed line); $S = 10$.

APPENDIX: SHORT-TIME EVOLUTION OF THE MAJORANA POINTS

1. Kerr dynamics

The evolution of the Majorana points for the Kerr Hamiltonian (3.1) is described by the following system of differential equations [36] :

$$\dot{z}_k = 2i\left[z_k^2\sum_{j\neq k}^{2S}\frac{1}{z_k - z_j} - z_k\left(S - \frac{1}{2}\right)\right], \quad \text{(A1)}$$

where $z_k(0) = 1$ for the initial spin coherent state $|\pi/2, 0\rangle$ and the derivative is taken over dimensionless time χt. Taking into account the parametrization of the antipodal points

$$\alpha_k = -\frac{1}{z_k^*} = -\tan\frac{\theta_k}{2}e^{i\phi_k}, \quad \text{(A2)}$$

$$\theta_k(0) = \pi/2, \quad \phi_k(0) = 0, \quad \text{(A3)}$$

we obtain the following equations for the angular variables:

$$\dot{\theta}_k = 4\sin^2\frac{\theta_k}{2}\text{Im}\left(e^{i\phi_k}\sum_{j\neq k}^{2S}\frac{1}{\alpha_j - \alpha_k}\right),$$

$$\dot{\phi}_k = 2\tan\frac{\theta_k}{2}\text{Re}\left(e^{i\phi_k}\sum_{j\neq k}^{2S}\frac{1}{\alpha_j - \alpha_k}\right) - 2S + 1. \quad \text{(A4)}$$

For the initial spin coherent states and short evolution times $\chi\tau \sim S^{-1}$ we should consider only a vicinity of the initial point (A3), so that $\theta_k = \frac{\pi}{2} + \xi_k$ and $\phi_k = \eta_k$, where $\xi_k, \eta_k \ll 1$. Expanding the denominator and the numerator in Eq. (A4) to the second and first order on ξ_k and η_k, respectively, we arrive at the following set of coupled equations for $\mu_k = \xi_k + i\eta_k$:

$$\dot{\mu}_k = 2i\sum_{j\neq k}\frac{1}{\mu_k - \mu_j} - i. \quad \text{(A5)}$$

The substitution $\mu_k = 2v_k\sqrt{i\chi\tau} - i\chi\tau$ leads to the *algebraic* equation

$$v_k = \sum_{j\neq k}\frac{1}{v_k - v_j}, \quad \text{(A6)}$$

which defines zeros of the Hermite polynomials $H_{2S}(v_k) = 0$. Finally, the approximate solutions of Eq. (A4) in the vicinity of $\theta_k(0) = \pi/2, \ \phi_k(0) = 0$ are

$$\theta_k \approx \frac{\pi}{2} + \sqrt{2}\chi\tau v_k, \quad \phi_k \approx (\sqrt{2}v_k - 1)\chi\tau, \quad \text{(A7)}$$

where only the roots $|v_k|/S \ll 1$ of the Hermite polynomial $H_{2S}(v)$ are considered. In Fig. 2(c) we plot the distribution of the antipodal Majorana points at the optimum time moment $\chi\tau \sim 0.021$. The points inside the sampling area $A(\Omega)$, which are 3σ of the spin fluctuations in the coherent state, are very well described by Eq. (A7).

2. Lipkin-Meshkov-Glik dynamics

The evolution of the Majorana points for the Hamiltonian (3.5) is described by

$$\dot{z}_k = \frac{i}{4 + 8s}\left[-2h(2s + 1)(z_k^2 - 1) - (2s - 1)(3z_k + z_k^3)\lambda + (1 + 6z_k^2 + z_k^4)\lambda\sum_{j\neq k}\frac{1}{z_k - z_j}\right]. \quad \text{(A8)}$$

Following the same steps as in the case of the Kerr Hamiltonian we arrive at the following set of equations for $\mu_k = \xi_k + i\eta_k$:

$$\dot{\mu}_k = -i\beta\mu_k + 4i\gamma\sum_{j\neq k}\frac{1}{\mu_k - \mu_j},$$

$$\beta = \frac{\lambda(2S - 1)}{2(2S + 1)} - h, \quad \gamma = \frac{\lambda}{2(2S + 1)}.$$

The approximate solution of the above equation for $h\tau \sim S^{-1}$,

$$\mu_k \approx e^{-i\beta\tau}2\sqrt{2i\gamma}\sqrt{\tau - i\beta\tau^2}v_k, \quad \text{(A9)}$$

where $H_{2S}(\nu_k) = 0$, leads to

$$\theta_k \approx \frac{\pi}{2} + \text{Re}(e^{-i\beta\tau}2\sqrt{2i\gamma\tau}\sqrt{1-i\beta\tau}\,\nu_k), \qquad \text{(A10)}$$

$$\phi_k \approx \text{Re}(e^{-i\beta\tau}2\sqrt{2i\gamma\tau}\sqrt{1-i\beta\tau}\,\nu_k), \qquad \text{(A11)}$$

where only those zeros of the Hermite polynomial $H_{2S}(\nu)$ that satisfy $|\nu_k|\sqrt{\gamma/S} \ll 1$ can be taken into account.

[1] M. V. Berry and K. E. Mount, Rep. Prog. Phys. **35**, 315 (1972); K. G. Kay, J. Chem. Phys. **100**, 4377 (1994); M. V. Berry and N. L. Balazs, J. Phys. A: Math. Gen. **12**, 625 (1979); R. G. Littlejohn, Phys. Rep. **138**, 193 (1986); V. P. Maslov and M. V. Fedoriuk, *Semi-Classical Approximation in Quantum Mechanics* (Springer Science & Business Media, 2001); M. C. Gutzwiller, *Chaos in Classical and Quantum Mechanics* (Springer-Verlag, New York, 1990); A. Voros, Prog. Theor. Phys. Suppl. **16**, 17 (1994).

[2] E. J. Heller, J. Chem. Phys. **65**, 1289 (1976); **67**, 3339 (1977); E. J. Heller, J. R. Remiers and J. Drolshangen, Phys. Rev. A **190**, 2613 (1987); M. J. Davis and E. J. Heller, J. Chem. Phys. **80**, 5036 (1984); P. Kinsler, M. Fernee, and P. D. Drummond, Phys. Rev. A **48**, 3310 (1993); V. G. Bagrov, V. V. Belov, and I. M. Ternov, Teor. Mat. Fiz. **50**, 390 (1982) [Theor. Mat. Phys. **50**, 256 (1982)]; P. Kinsler and P. D. Drummond, Phys. Rev. A **44**, 7848 (1991); G. Drobny and I. Jex, *ibid.* **46**, 499 (1992).

[3] L. S. Schulman, *Techniques and Applications of Path Integration* (Wiley, New York, 1981); M. S. Marinov, Phys. Lett. A **153**, 5 (1991).

[4] F. Gottwald and S. D. Ivanov, Chem. Phys. **503**, 77 (2018).

[5] W. H. Miller, J. Phys. Chem. A **105**, 2942 (2001); Adv. Chem. Phys. **25**, 69 (1974); K. G. Kay, Annu. Rev. Phys. Chem. **56**, 255 (2005).

[6] S. Garashchuk and V. A. Rassolov, Chem. Phys. Lett. **364**, 562 (2002); C. L. Lopreore and R. E. Wyatt, Phys. Rev. Lett. **82**, 5190 (1999); A. Donoso and C. C. Martens, *ibid.* **87**, 223202 (2001); S. Koda, J. Chem. Phys. **143**, 244110 (2015).

[7] E. Kluk, M. F. Herman, and H. L. Davis, J. Chem. Phys. **84**, 326 (1986); W. H. Miller, Mol. Phys. **100**, 397 (2002).

[8] M. Boiron and M. Lombardi, J. Chem Phys. **108**, 3431 (1998); H. Pal, M. Vyas, and S. Tomsovic, Phys. Rev. E **93**, 012213 (2016); W. Koch and D. J. Tannor, Chem. Phys. Lett. **683**, 306 (2017).

[9] F. Schroeck and E. Franklin, *Quantum Mechanics on Phase Space* (Kluwer, Dordrecht, 1996); W.-P. Schleich, *Quantum Optics in Phase Space* (Wiley, New York, 2001); C. K. Zachos, D. B. Fairle, and T. L. Curtright, *Quantum Mechanics in Phase Space* (World Scientific, Singapore, 2005); A. M. O. de Almeida, Phys. Rep. **295**, 265 (1998).

[10] J. E. Moyal, Proc. Cambridge Philos. Soc. **45**, 99 (1949).

[11] M. V. Berry, Philos. Trans. R. Soc. London, Ser. A **287**, 237 (1977).

[12] P. Ehrenfest, Z. Phys. **45**, 455 (1927); G. M. Zaslavsky, Phys. Rep. **80**, 157 (1981); G. A. Hagedorn and A. Joye, Ann. Henri Poincare **1**, 837 (2000); P. G. Silvestrov and C. W. J. Beenakker, Phys. Rev. E **65** 035208(R) (2002); R. Schubert, O. Vallejos, and F. Toscano, J. Phys. A: Math. Theor. **45**, 215307 (2012).

[13] V. S. Filinov, M. Bonitz, A. Filinov, and V. O. Golubnychiy, Lect. Notes Phys. **739**, 41 (2008).

[14] G. Schubert, V. S. Filinov, K. Matyash, R. Schneider, and H. Fehske, Int. J. Mod. Phys. C **20**, 1155 (2009).

[15] A. Polkovnikov, Ann. Phys. **325**, 1790 (2011).

[16] O. Steuernagel, D. Kakofengitis, and G. Ritter, Phys. Rev. Lett. **110**, 030401 (2013); M. Oliva, D. Kakofengitis, and O. Steuernagel, Phys. A (Amsterdam) **502**, 201 (2017); M. Oliva and O. Steuernagel, Phys. Rev. A **99**, 032104 (2019).

[17] T. Dittrich, C. Viviescas, and L. Sandoval, Phys. Rev. Lett. **96**, 070403 (2006); T. Dittrich, E. A. Gómez, and L. A. Pachón, J. Chem. Phys. **132**, 214102 (2010); R. N. P. Maia, F. Nicacio, R. O. Vallejos, and F. Toscano, Phys. Rev. Lett. **100**, 184102 (2008); F. Toscano, R. O. Vallejos, and D. Wisniacki, Phys. Rev. E **80**, 046218 (2009); S. Tomsovic, P. Schlagheck, D. Ullmo, J.-D. Urbina, and K. Richter, Phys. Rev. A **97**, 061606(R) (2018); G. M. Lando, R. O. Vallejos, G.-L. Ingold, and A. M. O. de Almeida, *ibid.* **99**, 042125 (2019).

[18] P. P. de M. Rios and A. M. Ozorio de Almeida, J. Phys. A: Math. Gen. **35**, 2609 (2002); A. M. Ozorio de Almeida and O. Brodier, Ann. Phys. **321**, 1790 (2006); A. M. Ozorio de Almeida, R. O. Vallejos, and E. Zambrano, J. Phys. A: Math. Theor. **46**, 135304 (2013).

[19] M. A. M. de Aguiar, S. A. Vitiello, and A. Grigolo, Chem. Phys. **370**, 42 (2010); T. F. Viscondi and M. A. M. de Aguiar, J. Math. Phys. **52**, 052104 (2011).

[20] G. Drobny, A. Bandilla, and I. Jex, Phys. Rev. A **55**, 78 (1997).

[21] J. P. Amiet and M. B. Ciblis, J. Phys. A: Math. Gen. **24**, 1515 (1991); A. B. Klimov, J. Math. Phys. **43**, 2202 (2002); A. B. Klimov and P. Espinoza, J. Opt. B **7**, 183 (2005); Y. P. Kalmykov, W.T. Coffey, and S. V. Titov, Adv. Chem. Phys. **161**, 41 (2016).

[22] A. B. Klimov, J. L. Romero, and H. de Guise, J. Phys. A: Math. Theor. **50**, 323001 (2017).

[23] A. B. Klimov, H. T. Dinani, Z. E. D. Medendorp, and H. de Guise, New J. Phys. **13**, 113033 (2012); H. Jeong, Y. D. Jho, and C. J. Stanton, Phys. Rev. Lett. **114**, 043603 (2015).

[24] K. Takahashi and A. Shudo, J. Phys. Soc. Jpn. **62**, 2612 (1993).

[25] W. K. Wootters, Ann. Phys. **176**, 1 (1987).

[26] J. Schachenmayer, A. Pikovski, and A. M. Rey, Phys. Rev. X **5**, 011022 (2015); New J. Phys. **17**, 065009 (2015); O. L. Acevedo, A. Safavi-Naini, J. Schachenmayer, M. L. Wall, R. Nandkishore, and A. M. Rey, Phys. Rev. A **96**, 033604 (2017); A. Piñeiro Orioli, A. Safavi-Naini, M. L. Wall, and A. M. Rey, *ibid.* **96**, 033607 (2017).

[27] L. Pucci, A. Roy, and M. Kastner, Phys. Rev. B **93**, 174302 (2016).

[28] B. Sundar, K. C. Wang, and K. R. A. Hazzard, Phys. Rev. A **99**, 043627 (2019).

[29] E. Majorana, Nuovo Cimento **9**, 43 (1932); H. Makela and H. Messina, Phys. Scr. T **140**, 014054 (2010); J. Crann, R. Pereira, and D. W. Kribs, J. Phys. A: Math. Theor. **43**, 255307 (2010); P. Kolenderski, Open Syst. Inf. Dyn. **17**, 107 (2010).

[30] R. L. Stratonovich, Zh. Eksp. Teor. Fiz. **31**, 1012 (1956) [Sov. Phys. JETP **4**, 891 (1957)]; G. S. Agarwal, Phys. Rev. A **24**, 2889 (1981); J. C. Várily and J. M. Garcia-Bondia, Ann. Phys. **190**, 107 (1989).

[31] D. A. Varshalovich, A. N. Moskalev, and V. K. Khersonskii,

Quantum Theory of Angular Momentum (World Scientific, Singapore, 1988).

[32] X. Suna and Z. Chenb, J. Approx. Theor. **151**, 186 (2008).

[33] J. Renes, R. Blume-Kohout, A. Scott, and C. Caves, J. Math. Phys. **45**, 2171 (2004); *Handbook of Combinatorial Designs*, 2nd ed., edited by C. J. Colbourn and J. H. Dinitz (CRC Press, Boca Raton, FL, 2007); A. Ambainis and J. Emerson, *Twenty-Second Annual IEEE Conference on Computational Complexity* (IEEE, Piscataway, NJ, 2007), p. 129,

[34] I. F. Valtierra, J. L. Romero, and A. B. Klimov, Ann. Phys. **383**, 620 (2017).

[35] P. Leboeuf and A. J. Voros, Phys. A: Math. Gen. **23**, 1765 (1990); S. Nonnenmacher and A. Voros, J. Phys. A: Math. Gen. **30**, 295 (1997); H. D. Liu and L. B. Fu, Phys. Rev. Lett. **113**, 240403 (2014); M. B. Cibils, Y. Cuche, P. Leboeuf, and W. F. Wreszinski, Phys. Rev. A **46**, 4560 (1992).

[36] P. Leboeuf, J. Phys. A: Math. Gen. **24**, 19 (1991).

[37] F. Yao, D. Li, H. Liu, L. Fu, and X. Wang, Sci. Rep. **7**, 15558 (2017); P. Ribeiro, J. Vidal, and R. Mosseri, Phys. Rev. Lett. **99**, 050402 (2007).

[38] M. Kitagawa and M. Ueda, Phys. Rev. A **47**, 5138 (1993).

[39] G. S. Agarwal, R. R. Puri, and R. P. Singh, Phys. Rev. A **56**, 2249 (1997).

[40] H. J. Lipkin, N. Meshkov, and A. J. Glick, Nucl. Phys. **62**, 188 (1965); **62**, 199 (1965); **62**, 211 (1965); R. Botet, R. Jullien, and P. Pfeuty, Phys. Rev. Lett. **49**, 478 (1982); R. Botet and R. Jullien, Phys. Rev. B **28**, 3955 (1983); J. I. Cirac, M. Lewenstein, K. Mølmer, and P. Zoller, Phys. Rev. A **57**, 1208 (1998).

[41] L. Chotorlishvili and A. Ugulava, Phys. D (Amsterdam) **239**, 103 (2010).